Dark Matter Phenomenology in the Non-Abelian Hidden Model

Juan Felipe Jiménez Román

Thesis Advisor: Dra. María Catalina Espinoza Hernández

Segundo Taller Más allá del Modelo Estándar y Astropartículas

Instituto de Física
Universidad Nacional Autónoma de México

29 septiembre 2025

Outline

1. Observational Evidence of Dark Matter
2. Dark Matter Model
3. Observables
4. Numerical Results
5. Conclusions

1. Observational Evidence of Dark Matter

Rotational Curves of Galaxies and Clusters

Fritz Zwicky (1933)[1]

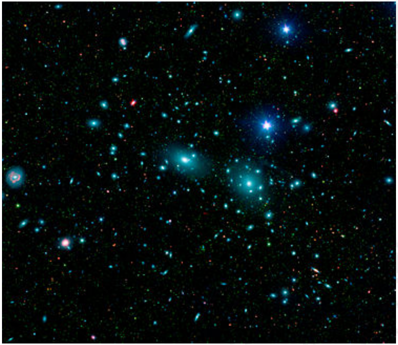

Figura 1: Cluster Coma ultraviolet and visible [3].

Vera Rubin (1970)[2]

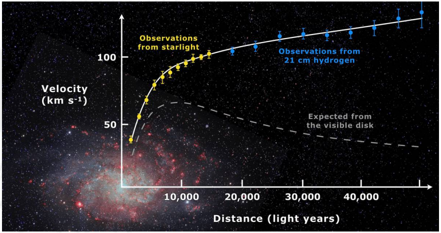

Figura 2: Galaxy Rotational Curve [4].

[1]Zwicky 1933, [2]Rubin et al. 1970, [3](GSFC) 2007, [4]Astrónomo.org 2024.

Dark Matter Properties

Properties of *DM* are the follow:

- Dark matter should not interact with photons, or its interaction should be extremely weak[1].
- The self- interaction of *DM* should be weak [2].
- Their barion interactions should be weak[2].
- Particles with velocities no-relativistic.
- Dark Matter should be a stable particle.
- Dark Matter can not be a standar model particle[2].

[1]Profumo et al. 2007, [2]D'Amico et al. 2009

2. Dark Matter Model

Dark Matter Model

Model Proposed by *Thomas Hambye* in 2009[1]

1. A local $SU(2)_{HS}$ symmetry was introduced in the *BSM* framework.

2. A scalar field Φ was added, which is a doublet under $SU(2)_{HS}$ and a singlet under the *SM*.

3. Through the Higgs mechanism, the gauge bosons A^i_μ acquire mass.

4. There is a global custodial symmetry $SU(2)_{CS}$ which stabilizes the gauge bosons A^i_μ, and their masses are degenerate.

Dark Matter Candidate

The three vector bosons A^i_μ.

5. The scalar η mixes with the Higgs boson, allowing the model to have possibilities for direct detection.

6. The model's phenomenology was analyzed through the direct detection cross section and the relic density.

[1] Hambye 2009

Model Lagrangiane

A local symmetry $SU(2)_{HS}$ was incorporated into the *BSM* framework. Moreover, a scalar field Φ was added, which transforms as a doublet under $SU(2)_{HS}$ and as a singlet under the *SM*[1].

$$\begin{aligned}\mathcal{L} = \mathcal{L}^{SM} - \frac{1}{4}F_a^{\prime\mu\nu}F_{\mu\nu}^{\prime a} + (D_\mu\Phi)^\dagger(D^\mu\Phi) \\ - \lambda_m\Phi^\dagger\Phi H^\dagger H - \mu_\phi^2\Phi^\dagger\Phi - \lambda_\phi(\Phi^\dagger\Phi)^2 - \mu H^\dagger H - \lambda(H^\dagger H)^2.\end{aligned} \quad (1)$$

- The kinetic term is given by $-\frac{1}{4}F^{\prime a\,\mu\nu}F_{\mu\nu}^{\prime a}$, where $F_{\mu\nu}^{\prime a} = \partial_\mu A_\nu^a - \partial_\nu A_\mu^a + \frac{g_\phi}{2}f^a{}_{bc}A_\mu^b A_\nu^c$.
- The covariant derivative is defined as $D_\mu\Phi = \partial_\mu\Phi - ig_\phi\frac{\tau_j}{2}A_\mu^j$.
- The terms $\mu_\phi^2\Phi^\dagger\Phi + \lambda_\phi(\Phi^\dagger\Phi)^2$ constitute the potential of Φ, analogous to the Higgs potential.
- The term $\lambda_m\Phi^\dagger\Phi\, H^\dagger H$ represents the coupling between the scalar doublet Φ and the Higgs doublet.

[1] Hambye 2009

Theoretical Constraints

Unitarity

Tree-level unitary scattering amplitude[1].

$$\lambda_m \leq 8\pi, \quad \lambda \leq 4\pi, \quad \lambda_\phi \leq 4\pi, \; 3(\lambda + \lambda_\phi) \pm \sqrt{9(\lambda + \lambda_\phi)^2 + 4\lambda_m^2} \leq 8\pi.$$

Mass Matrix

The scalar masses should be real [1]:

$$\lambda > 0, \quad \lambda_\phi > 0, \quad 2\lambda_m + \sqrt{\lambda\lambda_\phi} > 0.$$

Stability and Perturvativity

- The potential should be bounded from below [1].
- Couplings must remain perturbative [1].
- The electroweak vacuum is stable up to the Planck scale[1].

$$\lambda > 0, \quad \lambda_\phi > 0, \quad \lambda\lambda_\phi > 0.$$

[1] Baouche et al. 2021

Custodial Symmetry

The scalar doublet is given by:

$$\Phi = \frac{1}{\sqrt{2}} \begin{bmatrix} \phi_1 + i\phi_2 \\ \phi_4 + i\phi_3 \end{bmatrix}. \tag{2}$$

The term $\Phi^\dagger \Phi$ is writing like:

$$\Phi^\dagger \Phi = \frac{1}{2}(\phi_1^2 + \phi_2^2 + \phi_3^2 + \phi_4^2) = \frac{1}{2} \sum_i^4 \phi_i^2. \tag{3}$$

This equation can be understood as the norm of a four-component vector, which exhibits a global rotational symmetry $SO(4)$[1].

[1] Schwartz 2013

Custodial Symmetry

When the field Φ acquires a *vev* v_ϕ, the local symmetry $SU(2)_{HS}$ is spontaneously broken. Since the *vev* must be neutral, we have $\phi_4 \to v_\phi + \eta'$[1].

$$\Phi = \frac{1}{\sqrt{2}} \begin{bmatrix} \phi^+ \\ \phi^0 \end{bmatrix} = \frac{1}{\sqrt{2}} \begin{bmatrix} \phi_1 + i\phi_2 \\ v_\phi + \eta' + i\phi_3 \end{bmatrix}. \tag{4}$$

The term $\Phi^\dagger \Phi$ is written as:

$$\Phi^\dagger \Phi = \frac{1}{2} \left(\sum_{i=1}^{3} \phi_i^2 + (\eta' + v_\phi)^2 \right), \tag{5}$$

That term preserves the global rotational symmetry $SO(3)$, whose Lie algebra is isomorphic to the group $SU(2)_{CS}$ (custodial symmetry)[1].

Masses Degenerate

The conservation law associated with the custodial symmetry **stabilizes the gauge bosons A_μ and ensures their masses remain degenerate**.

[1] Schwartz 2013

Hypercharge Coupling

Starting from the Lagrangian of the hypercharge coupling, the **Dirac** spinors can be written in terms of their chiral components.

$$\Psi = \begin{bmatrix} \psi_L \\ \psi_R \end{bmatrix}, \tag{6}$$

Therefore, the Lagrangian of the hypercharge coupling interaction is:

$$\mathcal{L}_{SM} \supset g'\hat{Y}\bar{\Psi}\gamma^\mu \Psi B_\mu = g'\hat{Y}_L\bar{\psi}_L\gamma^\mu\psi_L B_\mu + g'\hat{Y}_R\bar{\psi}_R\gamma^\mu\psi_R B_\mu, \tag{7}$$

However, the operator $\hat{Y}$ assigns different eigenvalues to the *spinor* Ψ according to its chirality.

Stability of Dark Matter Candidate

Therefore, the hypercharge coupling breaks the global $SU(2)$ symmetry in the *SM*. **As a result, there are no interactions between the *DM* particles A^i_μ and the fermions of the *SM*[1].**

[1]Hambye 2009

Modelo

Apply the **unitary norm**:

$$\Phi = \frac{1}{\sqrt{2}} \begin{bmatrix} \phi_1 + i\phi_2 \\ \phi_4 + i\phi_3 \end{bmatrix} \to \frac{1}{\sqrt{2}} \begin{bmatrix} 0 \\ v_\phi + \eta' \end{bmatrix}. \tag{8}$$

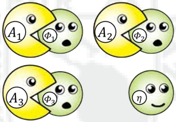

Figura 3: The gauge bosons acquire mass through the action of the Goldstone bosons.

Replacing the new doublet, the Lagrangian in the interaction basis is as follows:

$$\begin{aligned} \mathcal{L} = \mathcal{L}^{SM} - \frac{1}{4} F'^{\mu\nu} F'_{\mu\nu} + \frac{1}{8}(g_\phi v_\phi)^2 A_\mu \cdot A^\mu + \frac{1}{8} g_\phi^2 A_\mu \cdot A^\mu \eta'^2 + \frac{1}{4} g_\phi^2 v_\phi A_\mu \cdot A^\mu \eta' \\ + \frac{1}{2}(\partial_\mu \eta')^2 - \frac{\lambda_m}{2}(\eta' + v_\phi)^2 H^\dagger H - \frac{\mu_\phi^2}{2}(\eta' + v_\phi)^2 - \frac{\lambda_\phi}{4}(\eta' + v_\phi)^4 \\ - \mu^2 H^\dagger H - \lambda(H^\dagger H). \end{aligned} \tag{9}$$

Mass Matrix

Considering the potential in the scalar sector:

$$V = V_{SM} + \frac{\lambda_m}{4}(\eta' + v_\phi)^2(h' + v)^2 + \frac{\mu_\phi^2}{2}(\eta' + v_\phi)^2 + \frac{\lambda_\phi}{4}(\eta' + v_\phi)^4 + \frac{\mu^2}{2}(h' + v)^2 + \frac{\lambda}{4}(h' + v)^4. \tag{10}$$

The mass matrix is obtained from:

$$(M^2)_{ij} = \frac{\partial^2 V}{\partial \phi_i \partial \phi_j}\Big|_{\phi=0}, \tag{11}$$

Hence, the mass matrix takes the following form:

$$M^2 = \begin{bmatrix} m_{h'}^2 & m_{h'\eta'}^2 \\ m_{h'\eta'}^2 & m_{\eta'}^2 \end{bmatrix} = \begin{bmatrix} \frac{\lambda_m v_\phi^2}{2} + 3\lambda v^2 + \mu^2 & \lambda_m v_\phi v \\ \lambda_m v_\phi v & \frac{\lambda_m v^2}{2} + 3\lambda_\phi v_\phi^2 + \mu_\phi^2 \end{bmatrix}, \tag{12}$$

From the diagonalization of this matrix, it is possible to obtain the **rotation matrix** of the scalar fields.

$$(M^2)_{ij} \rightarrow \tan 2\beta.$$

Lagrangian in the Physical Basis

The two scalars in the interaction basis mix according to the following matrix:

$$\begin{bmatrix} h \\ \eta \end{bmatrix} = \begin{bmatrix} \cos\beta & -\sin\beta \\ \sin\beta & \cos\beta \end{bmatrix} \cdot \begin{bmatrix} h' \\ \eta' \end{bmatrix}. \tag{13}$$

Therefore, the Lagrangian in the **physical basis** is given by:

$$\begin{aligned} \mathcal{L} = \mathcal{L}_{SM} - \frac{1}{4}F'_{\mu\nu}F'^{\mu\nu} + \frac{1}{8}(g_\phi v_\phi)^2 A_\mu A^\mu + \frac{1}{2}(\partial_\mu \eta)^2 + \frac{1}{2}(\partial_\mu h)^2 - \frac{1}{2}m_\eta^2\eta^2 \\ - \frac{1}{2}m_h^2 h^2 + A_\mu A^\mu \left[{\kappa_\eta}^\phi \eta^2 + {\kappa_h}^\phi h^2 + {\kappa_{\eta h}}^\phi \eta h + 2v_\phi {\xi_\eta}^\phi \eta + 2v_\phi {\xi_h}^\phi h\right] \\ \left[2{W_\mu}^+ W^{-\mu} + \frac{1}{\cos^2\theta_w} Z_\mu Z^\mu\right]\left[\kappa_\eta \eta^2 + \kappa_h h^2 + \kappa_{\eta h}\eta h + 2v\xi_\eta \eta + 2v\xi_h h\right] \\ - \lambda_\eta \eta^4 - \lambda_h h^4 - \lambda_1 \eta^2 h^2 - \lambda_2 \eta h^3 - \lambda_3 \eta^3 h - \rho_\eta \eta^3 - \rho_h h^3 - \rho_1 \eta^2 h - \rho_2 \eta h^2 \\ - (h\cos\beta + \eta\sin\beta)\sum_f \left(\frac{m_f}{v}\bar{f}f\right). \end{aligned} \tag{14}$$

3. Observables

Direct Detection

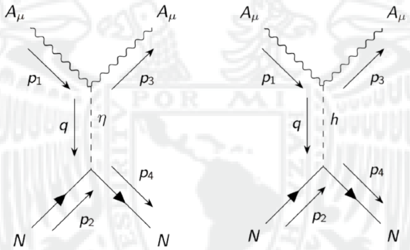

Figura 4: Elastic scattering between a *DM* particle and a nucleon

The cross section is shown below:

$$\sigma^{SI} = \frac{1}{64\pi} f^2 g_\phi^4 \sin^2 2\beta m_N^2 \frac{v_\phi^2}{v^2} \frac{(m_\eta^2 - m_h^2)^2}{m_\eta^4 m_h^4} \left(\frac{m_N}{m_A + m_N} \right)^2 . \tag{15}$$

Relic Density

The relic density is defined as follows:

$$\Omega_x^o = \frac{\rho_x}{\rho_c^o} = \frac{n_{x+\overline{x}} m_x}{\rho_c^o}, \tag{16}$$

where $n_{x+\overline{x}} = \frac{N_{x+\overline{x}}}{V}$ y $\rho_c^o = \frac{3H_o^2}{8\pi G_N} = (1.05371 \times 10^{-5}\, \text{GeV cm}^{-3})$ [1].

The relic density of a species evolves according to three different stages:

- **Stage I:** The system enters thermal equilibrium[2].
- **Stage II:** The system is in equilibrium and decouples (Freeze-out)[1].
- **Stage III:** The system is out of equilibrium[1].

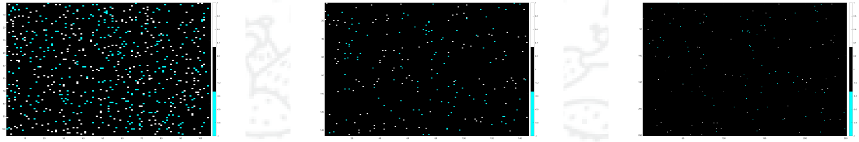

Figura 5: Relic Density Across Three Different Stages

[1]Giunti et al. 2007, [2]Rubakov et al. 2017

5.Numerical Results

Data Analysis

A likelihood profile has been built in the parameter space based on the following contributions:

$$\mathcal{L} = \mathcal{L}_{\Omega} + \mathcal{L}_{m_h} + \mathcal{L}_{\sigma}, \tag{17}$$

donde:

- $\mathcal{L}_{\Omega}$ is the likelihood function related to the relic density measurement from the **PLANCK** experiment and calculated using `MicrOMEGAs`.
- $\mathcal{L}_{m_h}$ is the likelihood function related to the Higgs boson mass, calculated using `HiggsSignals`.
- $\mathcal{L}_{\sigma}$ is the likelihood function related to the experimental cross section data, calculated using `DDCalc`.

For the Case of the Relic Density

In this case, $\mathcal{L}_{\Omega}$ was not considered to avoid biasing the results.

Relic Density

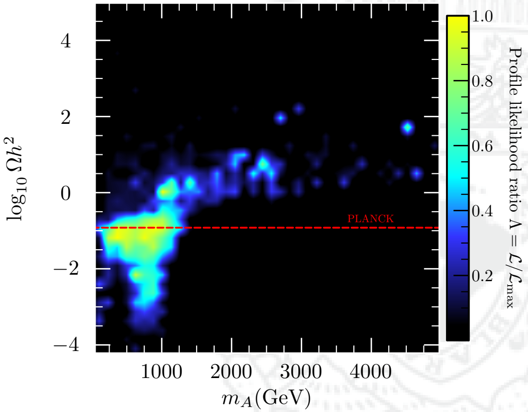

- The region of the mass of A_μ^i that maximizes the likelihood is $m_A \in [60, 1390]$ GeV.
- Masses above $m_A > 1390$ GeV are excluded.

Figura 6: Likelihood ratio as a function of the mass of the dark matter candidate (m_A) and the relic density, compared to the Planck density $\Omega h^2 = 0.120 \pm 0.001$ (red dashed line)[1].

[1] Aghanim et al. 2020

Direct Detection Cross Section

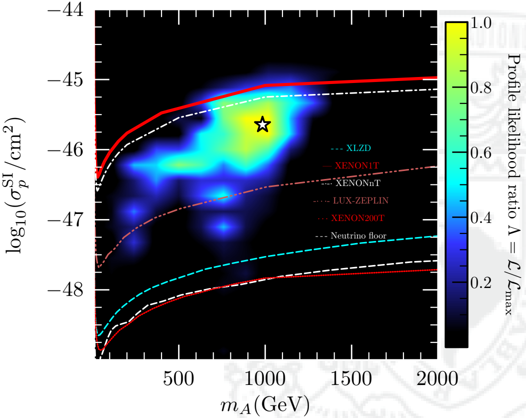

- The best-fit point is located around $m_A \approx 1000$ GeV.

Figura 7: Likelihood ratio as a function of the dark matter candidate mass (m_A) and the spin-independent direct detection cross section $\log(\sigma_p^{SI}/\text{cm}^2)$[1,2,3,4], with current data from the LUX-ZEPLIN experiment (2024)[5] and considering the XLZD project[6].

[1]Aprile et al. 2023, [2]Aprile et al. 2018, [3]Billard et al. 2014, [4]Schumann et al. 2015, [5]Aalbers et al. 2024, [6]Collaboration et al. 2024

Coupling Constant

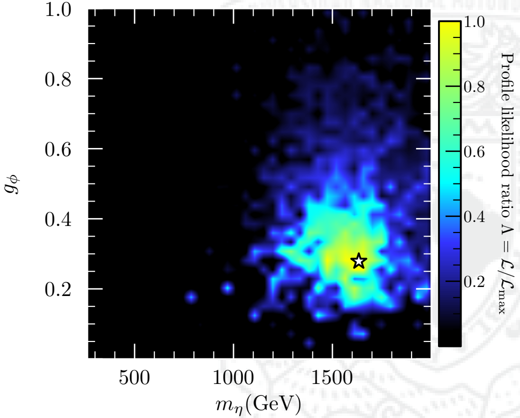

- The mass region of η that maximizes the likelihood is $m_\eta \in [1200, 1790]$ GeV.
- The best-fit point is around $m_\eta \approx 1630$ GeV.
- The gauge coupling constant region that maximizes the likelihood is $g_\phi \in [0.14, 0.48]$.

Figura 8: Likelihood ratio as a function of the coupling constant (g_ϕ) and the mass of the additional scalar (m_η), showing the best-fit region for these variables.

Annihilation Channels

The scattering amplitudes were computed as functions of the *Mandelstam* variables t and s, with the goal of determining the dominant annihilation channel at each point in the parameter space[1]:

$$\sigma_i(s) = \frac{1}{16\pi\lambda(s, m_a^2, m_b^2)} \int_{t^-}^{t^+} dt\, |\mathcal{M}_i|^2 \,, \tag{18}$$

where the integration limits for an arbitrary process $a + b \to c + d$ are given by[1]:

$$t^{\pm} = m_a^2 + m_c^2 - \frac{1}{2s}\left[(s + m_a^2 - m_b^2)(s + m_c^2 - m_d^2) \mp \lambda^{1/2}(s, m_a^2, m_b^2)\, \lambda^{1/2}(s, m_c^2, m_d^2)\right] , \tag{19}$$

and the kinematic function λ is defined as $\lambda(x, y, z) = (x - y - z)^2 - 4yz$. Finally, the thermally averaged rate for channel i is given by[2]:

$$\gamma_i = \frac{T}{64\pi^4} \int_{4m_A^2}^{\infty} ds \sqrt{s}\, K_1\left(\frac{\sqrt{s}}{T}\right) \hat{\sigma}_i(s). \tag{20}$$

[1]Byckling et al. 1971, [2]Cirelli et al. 2007

Annihilation Channels

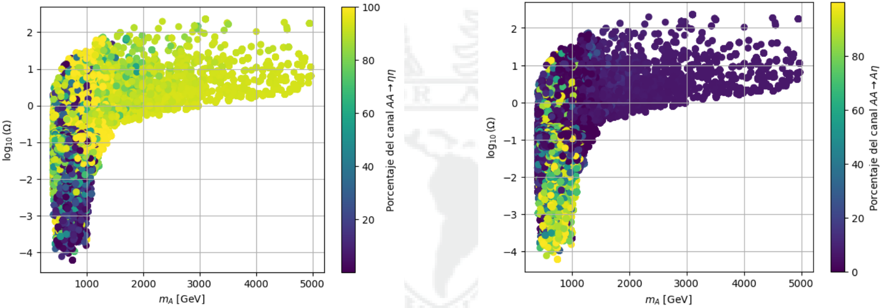

(a) Channel $A_\mu + A_\mu \to \eta + \eta$ (b) Channel $A_\mu + A_\mu \to A_\mu + \eta$

Figura 9: Parameter space of the relic density, highlighting the dominant annihilation channels.

6. Conclusions

Conclusions

- There is a parameter space where the model exactly predicts the observed relic density, confirming its viability.
- The parameter space that satisfies all theoretical constraints lies above the neutrino floor, suggesting theoretical prospects for direct detection.
- A significant fraction of the parameter space can be explored by LUX-ZEPLIN experiments, while practically the entire space is accessible to the XENON200T experiment.
- Recent results from LUX-ZEPLIN in 2024 indicate that over 90 % of the favored parameter space region is accessible with this experiment.
- The future XLZD experiment has the potential to fully probe the favored region of the parameter space.

Outlook

- Constrain the parameter space by considering indirect detection data.
- Explore detection processes through particle collider experiments.
- Study the model's behavior at energy scales significantly higher than the electroweak vacuum scale.

Thank You Very Much

7. References

References I

(GSFC), N. /. J.-C. /. L. J. (2007). *Dwarf Galaxies in the Coma Cluster*. URL: http://www.spitzer.caltech.edu/images/1803-ssc2007-10a1-Dwarf-Galaxies-in-the-Coma-Cluster.

Aalbers, J. et al. (2024). *Dark Matter Search Results from 4.2 Tonne-Years of Exposure of the LUX-ZEPLIN (LZ) Experiment*. arXiv: 2410.17036 [hep-ex]. URL: https://arxiv.org/abs/2410.17036.

Aghanim, N. et al. (2020). "Planck 2018 results. VI. Cosmological parameters". En: *Astron. Astrophys.* 641. [Erratum: Astron. Astrophys. 652, C4 (2021)], A6. DOI: 10.1051/0004-6361/201833910. arXiv: 1807.06209 [astro-ph.CO].

Aprile, E. et al. (2018). "Dark Matter Search Results from a One Ton-Year Exposure of XENON1T". En: *Phys. Rev. Lett.* 121.11, pág. 111302. DOI: 10.1103/PhysRevLett.121.111302. arXiv: 1805.12562 [astro-ph.CO].

References II

Aprile, E. et al. (2023). "First Dark Matter Search with Nuclear Recoils from the XENONnT Experiment". En: *Phys. Rev. Lett.* 131.4, pág. 041003. DOI: 10.1103/PhysRevLett.131.041003. arXiv: 2303.14729 [hep-ex].

Astrónomo.org (2024). *Rotación Galáctica: repaso de conceptos y evidencia materia oscura*. URL: https://www.astronomo.org/foro/index.php?topic=38520.0 (visitado 01-04-2025).

Baouche, N. et al. (2021). "Phenomenology of the hidden SU(2) vector dark matter model". En: *Phys. Rev. D* 104.7, pág. 075022. DOI: 10.1103/PhysRevD.104.075022. arXiv: 2105.14387 [hep-ph].

Billard, J. et al. (2014). "Implication of neutrino backgrounds on the reach of next generation dark matter direct detection experiments". En: *Phys. Rev. D* 89.2, pág. 023524. DOI: 10.1103/PhysRevD.89.023524. arXiv: 1307.5458 [hep-ph].

References III

Byckling, E. et al. (1971). *Particle Kinematics: (Chapters I-VI, X)*. Jyvaskyla, Finland: University of Jyvaskyla.

Cirelli, M. et al. (2007). "Cosmology and Astrophysics of Minimal Dark Matter". En: *Nucl. Phys. B* 787, págs. 152-175. DOI: 10.1016/j.nuclphysb.2007.07.023. arXiv: 0706.4071 [hep-ph].

Collaboration, X. et al. (2024). *The XLZD Design Book: Towards the Next-Generation Liquid Xenon Observatory for Dark Matter and Neutrino Physics*. arXiv: 2410.17137 [hep-ex]. URL: https://arxiv.org/abs/2410.17137.

D'Amico, G. et al. (2009). *Dark Matter Astrophysics*. arXiv: 0907.1912 [astro-ph.CO].

Giunti, C. et al. (mar. de 2007). *Fundamentals of Neutrino Physics and Astrophysics*. Oxford University Press. ISBN: 9780198508717. DOI: 10.1093/acprof:oso/9780198508717.001.0001. URL: https://doi.org/10.1093/acprof:oso/9780198508717.001.0001.

References IV

Hambye, T. (2009). "Hidden vector dark matter". En: *JHEP* 01, pág. 028. DOI: 10.1088/1126-6708/2009/01/028. arXiv: 0811.0172 [hep-ph].

Profumo, S. et al. (ene. de 2007). "Shadow of dark matter". En: *Phys. Rev. D* 75 (2), pág. 023521. DOI: 10.1103/PhysRevD.75.023521. URL: https://link.aps.org/doi/10.1103/PhysRevD.75.023521.

Rubakov, V. A. et al. (2017). *Introduction to the Theory of the Early Universe: Hot big bang theory*. Singapore: World Scientific. ISBN: 978-981-320-987-9, 978-981-320-988-6, 978-981-322-005-8. DOI: 10.1142/10447.

Rubin, V. C. et al. (feb. de 1970). "Rotation of the Andromeda Nebula from a Spectroscopic Survey of Emission Regions". En: 159, pág. 379. DOI: 10.1086/150317.

References V

Schumann, M. et al. (2015). "Dark matter sensitivity of multi-ton liquid xenon detectors". En: *JCAP* 10, pág. 016. DOI: 10.1088/1475-7516/2015/10/016. arXiv: 1506.08309 [physics.ins-det].

Schwartz, M. D. (2013). *Quantum Field Theory and the Standard Model*. Cambridge: Cambridge University Press.

Zwicky, F. (1933). "Die Rotverschiebung von extragalaktischen Nebeln". En: *Helv. Phys. Acta* 6, págs. 110-127. DOI: 10.1007/s10714-008-0707-4.